

Synthesis, in vitro, and in vivo characterization of an integrin $\alpha_v\beta_3$ -targeted molecular probe for optical imaging of tumor

Christopher A. Burnett,^{a,†} Jianwu Xie,^{a,†} Jade Quijano,^a Zhimin Shen,^b Finie Hunter,^a Monica Bur,^a King C. P. Li^a and S. Narasimhan Danthi^{a,*}

^aMolecular Imaging Laboratory, Clinical Center, National Institutes of Allergies and Infectious Diseases, National Institutes of Health, 10 Center Drive, Bethesda, MD 20892, USA

^bVaccine Research Center, National Institutes of Health, 40 Convent Drive, Bethesda, MD 20892, USA

Received 23 December 2004; revised 8 March 2005; accepted 11 March 2005

Available online 6 April 2005

Abstract—Integrin $\alpha_v\beta_3$ is a widely-recognized target for the development of targeted molecular probes for imaging pathological conditions. $\alpha_v\beta_3$ is a cell-surface receptor protein that is upregulated in various pathological conditions including osteoporosis, rheumatoid arthritis, macular degeneration, and cancer. The synthesis of an $\alpha_v\beta_3$ -targeted optical probe **7** from compound **1**, and its in vitro and in vivo characterization is described. A series of aliphatic carbamate derivatives of the potent non-peptide integrin antagonist **1** was synthesized and the binding affinity to $\alpha_v\beta_3$ was determined in both enzyme linked immunosorbent assay (ELISA) and cell adhesion inhibition assays. The hydrophobic carbamate-linked appendages improved the binding affinity of the parent compound for $\alpha_v\beta_3$ by 2–20 times. A Boc-protected neopentyl derivative in the series is shown to have the best binding affinity to $\alpha_v\beta_3$ ($IC_{50} = 0.72$ nM) when compared to compound **1** as well as to *c*-RGDfV. Optical probe **7** utilizes the neopentyl linker and demonstrates increased binding affinity and significant tumor cell uptake in vitro as well as specific tumor accumulation and retention in vivo. These results illustrate the potential of employing integrin-targeted molecular probes based on **1** to image a multitude of diseases associated with $\alpha_v\beta_3$ overexpression. Published by Elsevier Ltd.

1. Introduction

The integrins are a family of cell-surface glycoproteins that mediate cell survival, proliferation, and cell migration through explicit non-covalent interactions with endogenous extra cellular matrix (ECM) proteins. To date, 19 alpha and 8 beta mammalian subunits have been identified in this class and their distinct pair-wise combinations consequently provide 25 unique heterodimeric transmembrane receptor proteins.¹ Investigations into the basic structure of the integrins utilizing electron microscopy² reveal that these proteins consist of a large *N*-terminal extra cellular domain, a membrane-spanning region, and a short cytoplasmic tail. The structure of the integrins allows them to function as bidirectional cellular signal transducers.³ Conformational changes in-

duced by ligand binding to integrins invoke signaling cascades inside the cell that regulate gene expression, activate kinases, and direct cytoskeletal organization.⁴ Alternatively, internal cellular activation can produce both conformational changes and multimeric clustering of the integrins, which results in non-constitutive binding to ligands, ECM components, as well as other cells.⁵ The type and degree of the signaling event is determined by the conformation and nature of the ligand and is regulated by divalent cations bound to metal ion-dependent adhesion sites on the integrin receptor.⁶

The vital role integrins play in fundamental cellular processes renders them as attractive targets for the development of treatments for a variety of diseases. Among the more prominent targets is the integrin $\alpha_v\beta_3$, which has been implicated in the formation of new blood vessels (angiogenesis) and tissue remodeling in major diseases such as osteoporosis,⁷ rheumatoid arthritis,⁸ macular degeneration,⁹ and cancer.¹⁰ The $\alpha_v\beta_3$ integrin receptor has also been shown to mediate the internalization of rotavirus¹¹ and adenovirus.¹² Integrin $\alpha_v\beta_3$ binds to

Keywords: Integrin $\alpha_v\beta_3$; Tumor; Molecular probe; Imaging.

* Corresponding author. Tel.: +1 301 451 5170; fax: +1 301 435 2714; e-mail: ndanthi@cc.nih.gov

[†] Both authors contributed equally.

the natural ligands vitronectin, fibrinogen, osteopontin, and bone sialoprotein by recognizing the amino acid sequence Arg-Gly-Asp (RGD).¹³ Several research groups have synthesized peptide and peptidomimetic small molecule antagonists based on this motif that demonstrate remarkable affinity and selectivity to $\alpha_v\beta_3$.¹⁴

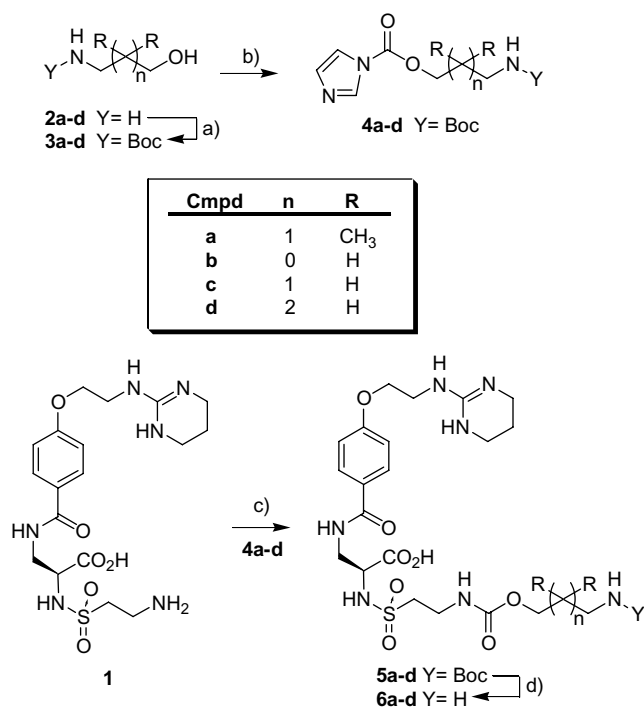
Targeting the integrin $\alpha_v\beta_3$ by directly interfering with its function is potentially a very effective strategy for the treatment of several diseases.¹⁵ Administration of small molecule antagonists of $\alpha_v\beta_3$ has been shown to reduce bone resorption in animal models of osteoporosis.¹⁶ The monoclonal antibody Vitaxin as well as the potent cyclic peptide *c*-[RGDf(N-Me)V] are currently in clinical trials for $\alpha_v\beta_3$ -targeted anti-angiogenic cancer therapy.¹⁷ Angiogenesis is a result of multiple biochemical pathways^{17a,18} and inhibiting solely $\alpha_v\beta_3$ might be a less effective strategy for anti-angiogenic therapy. Recently, the integrin antagonist **1** (Scheme 1) was employed as the targeting agent for targeted gene delivery to tumor neovasculature.¹⁹ Transfection of a mutant *Raf* gene to the tumor associated endothelium led to tumor cell apoptosis and regression of primary and metastatic tumors in M21 tumor-bearing mice. Research in our laboratory is focused on developing $\alpha_v\beta_3$ -targeted low molecular weight compounds and nanoparticle based therapeutic materials as well as imaging probes. Apart from the prospective use of the $\alpha_v\beta_3$ antagonists as anti-angiogenic agents, we are also developing novel delivery systems that use $\alpha_v\beta_3$ antagonists as targeting agents while simultaneously carrying a payload for

imaging or therapy. The payloads include fluorescent dyes for optical imaging, gadolinium complexes for MRI, ¹¹¹In complexes for SPECT, ¹⁸F-labeled probes for PET, as well as cytotoxic agents or genes for therapy. Several research groups have demonstrated the utility of coupling peptide or peptidomimetic ligands of $\alpha_v\beta_3$ to molecular beacons for use in non-invasive *in vivo* imaging of tumor-related angiogenesis.^{20–23} ¹⁸F-labeled RGD-containing cyclic peptides have been applied as PET probes.²⁰ DOTA-conjugated non-peptide integrin antagonists chelating ¹¹¹In or ⁹⁰Y have been used for $\alpha_v\beta_3$ -targeted SPECT imaging as well as therapy, respectively.²¹ MRI probes have been developed for *in vivo* imaging of tumor models in animals by attaching $\alpha_v\beta_3$ specific antibodies to paramagnetic nanoparticles.²² Most recently, several research groups have prepared $\alpha_v\beta_3$ -targeted near-infrared probes utilizing the cyclic peptide *c*-RGDyK as the targeting agent for optical imaging *in vivo*.²³ In this paper we describe the synthesis of novel carbamate linkers of a known integrin antagonist **1** and also the synthesis, *in vitro*, and *in vivo* characterization of an integrin $\alpha_v\beta_3$ probe **7** derived from compound **1**. Compound **7** represents the first example of a non-peptide integrin $\alpha_v\beta_3$ -targeted optical probe. The convergent synthesis of **1**, a nanomolar inhibitor of $\alpha_v\beta_3$, has been previously described as a component of a liposomal-based nanoparticle system.¹⁹ The centrally-constrained benzoylamino-3-propionic acid scaffold originally developed by Duggan et al.²⁴ provides optimum spacing between the acidic and basic portions of this RGD mimic. Previous work demonstrated that when the amine **1** was attached to a nanoparticle system through an amide linkage, it retained significant binding affinity to $\alpha_v\beta_3$ after conjugation, however extensive structure–activity studies on the amine terminus of **1** were not examined.¹⁹ The current study focuses on determining the structure–activity relationship potential at the ethylamine terminus of the molecule and exploiting this potential by attaching a molecular beacon for optical imaging. Herein, we describe the synthesis of a series of aliphatic carbamate derivatives of **1** that have enhanced binding affinity for $\alpha_v\beta_3$ and the development of an integrin-targeted optical probe **7**, synthesized from **6a**, for *in vivo* tumor imaging. The *in vitro* binding affinity of **7** for $\alpha_v\beta_3$ and the *in vivo* biodistribution of **7** in a mouse melanoma model are also described.

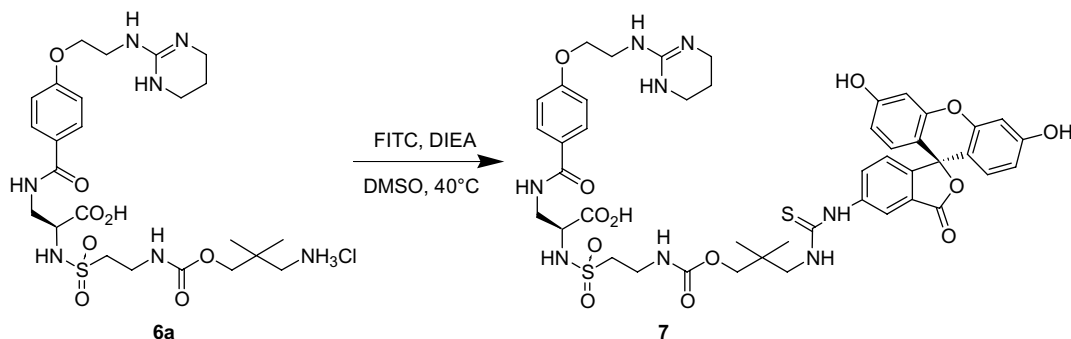
2. Results and discussion

2.1. Synthesis of carbamate-linked derivatives

The synthesis of the carbamate-linked derivatives of **1** (Scheme 1) begins with commercially available amino alcohols **2a–d**. The amines were first protected as their *t*-butoxycarbonyl derivatives **3a–d** by the method described by Ensich and Hesse,²⁵ and their purity was verified by NMR.²⁶ Protection was followed by activation of the alcohols as monocarbonylimidazoles **4a–d**. The activated alcohols were then coupled to the free amine **1** in DMSO to provide carbamates **5a–d**. In each case, selective deprotection of the Boc carbamate in the presence of neopentyl, ethyl, propyl, or butyl carbamate was



Scheme 1. Synthesis of compounds. Reagents and conditions: (a) (Boc)₂O, Et₃N, CH₂Cl₂; (b) 1,1'-carbonylimidazole, DIEA, CH₂Cl₂; (c) DIEA, DMSO, 70 °C; (d) 4 M HCl, dioxane, 0 °C. Yield **5a–d**: 66%, 23%, 36%, and 33%, respectively. Compounds **6a–d** were obtained as hydrochloride salts in quantitative yield.



Scheme 2. Synthesis of compound 7.

achieved with anhydrous HCl in dioxane at 0 °C to provide amines **6a–d**. Following lyophilization, no appreciable amount of unreacted **1** was detected after deprotection reactions.²⁷ Compound **7** was synthesized (Scheme 2) by reacting the amine **6a** and the commercially available fluorescein isothiocyanate. All intermediates and final compounds were characterized by ¹H NMR, ¹³C NMR, and high-resolution mass spectrometry.

2.2. In vitro binding affinity assay

The integrin antagonist compounds were evaluated for their ability to competitively inhibit the attachment of the natural ligand vitronectin to purified human $\alpha_v\beta_3$ by ELISA and $\alpha_v\beta_3$ -expressing M21 melanoma cells in cell adhesion assays. ELISA measured competitive binding of the integrin antagonist and biotinylated human vitronectin for the immobilized receptor $\alpha_v\beta_3$. For cell adhesion assays, the M21 cells were first incubated with the integrin antagonists then subsequently added to 96-well plates previously coated with human vitronectin. Inhibition of cell adhesion efficiency was measured by the detection of the remaining cells stained with crystal violet after plate washing. The results are summarized in Table 1. Inhibition of cell adhesion is expressed as a ratio (*Q*) relative to the parent compound **1** due to the inherent variability of the cells used in the assay. The re-

sults of both the ELISA and cell adhesion assays show that the aliphatic carbamate derivatives of the parent compound **1** had equal or increased binding affinity for $\alpha_v\beta_3$. In the ELISA, the Boc-protected neopentyl derivative **5a** had an IC₅₀ of 0.72 nM compared to 14.1 nM for compound **1**. The propyl derivative **5c**, which had the same chain length but less steric bulk than **5a** had only slightly decreased activity.

Deprotection to reveal the terminal amine resulted in a net decrease in activity for all four linker lengths studied, however the neopentyl **6a** retained superior activity in this free amine series. The most conspicuous decrease in activity is observed for the deprotection of the propyl derivative indicating the geminal methyl groups of the neopentyl derivatives favor interaction with the receptor. The trends observed in the ELISA are mirrored in the cell adhesion assay results. Most notable is the dramatic increase in activity seen for **5a** when compared to **1**. This is particularly encouraging as the cell adhesion assay is designed to more closely resemble activity in vivo when compared to the ELISA. Furthermore, both neopentyl derivatives **5a** and **6a** show superior $\alpha_v\beta_3$ binding affinity when compared to the potent cyclic peptide *c*-[RGDFV] in our assay system.

2.3. In vitro fluorescence microscopy

Further studies with fluorescence microscopy were used to determine the cellular distribution of **7** in the context of $\alpha_v\beta_3$ -expressing cells (M21) in vitro. The M21 cells were incubated for 5 min following the addition of 500 μ L of **7** (50 μ g/mL). Cells were mounted and counterstained with 4',6-diamidino-2-phenylindole (DAPI) to delineate the vessels and observed with fluorescence microscopy. Negative controls were given the same concentration of FITC only. Figure 1 summarizes the results, which suggest that the signal from **7** is found on the cell membrane surface compared to controls, which demonstrate non-specific accumulation of FITC outside the cell.

2.4. In vivo tumor accumulation and biodistribution

Optical imaging of excised organs was accomplished by using a multispectral imaging system using tunable filter technology optically coupled to a CCD to generate

Table 1. In vitro evaluation of carbamate-linked integrin antagonists

Comps	R	n	Y	ELISA IC ₅₀ , nM ^a	Cell adhesion <i>Q</i> ^b
1	—	—	—	14.1 (±1.4)	—
5a	CH ₃	1	—CO ₂ C(CH ₃) ₃	0.72 (±0.08)	65.8
5b	H	0	—CO ₂ C(CH ₃) ₃	1.70 (±0.20)	5.8
5c	H	1	—CO ₂ C(CH ₃) ₃	1.02 (±0.12)	22.8
5d	H	2	—CO ₂ C(CH ₃) ₃	1.34 (±0.14)	4.7
6a	CH ₃	1	H	2.94 (±0.19)	5.4
6b	H	0	H	3.64 (±0.30)	4.0
6c	H	1	H	6.68 (±0.54)	3.9
6d	H	2	H	3.13 (±0.33)	1.8
7	CH ₃	1	Fluorescein	3.4 (±0.33)	—
<i>c</i> -[RGDFV] ^c	—	—	—	6.41 (±0.49)	—

^a Values are averages of at least three determinations.

^b Ratio of the IC₅₀ of **1** to test compound per individual determination.

^c Purchased from Bachem Bioscience.

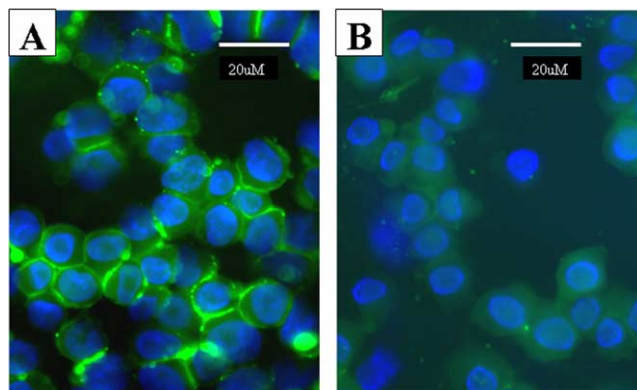


Figure 1. Bar represents 20 μM . Fluorescence microscopy of in vitro cell assay of compound **7** and FITC. M21 human melanoma cells expressing $\alpha_v\beta_3$ were cultured in glass chambers. Cells were given fresh media 30 min prior to treatment. Compound **7** (500 μL , 50 $\mu\text{g}/\text{mL}$) was added to each glass chamber and left to incubate for 5 min. Cells were washed with warm PBS three times and subsequently mounted, counterstained with DAPI and observed under a fluorescence microscope. Control chambers were given the same concentration of FITC without compound **7**. Signal from compound **7** is present on the cell membrane surface compared to controls, which demonstrate non-specific accumulation of FITC signal outside the cell. (A) Cell uptake of compound **7**; (B) cell uptake of the negative control FITC.

multispectral data. During image acquisition, FITC was characteristically excited at 494 nm although emission data were collected from 500 to 950 nm including data from FITC's characteristic emission at 518 nm. Because fluorescein derivatives are best suited for imaging superficial tissues due to the shallow penetration of blue light in tissue, tumors and various organs were excised to obtain more accurate biodistribution data.²⁸ For in vivo optical imaging, the M21 cells were injected into the right flanks of mice and allowed to grow for 14–21 days into a palpable mass. Compound **7** was injected into the lateral tail vein of M21 tumor-bearing mice. Controls were M21 tumor-bearing mice that received no injection. Preferential retention of the agent in the tumor was fast and showed marked signal in the tumor at 30 min compared to other organs. The signal remained pronounced in the tumor and showed decreased signal in the liver at 4 h. The results are summarized in Figure 2. Qualitative data from the images in Figure 2 are summarized in Figure 3. At 30 min, the signal intensity in the tumor is nearly three times that found in the liver and muscle. At 4 h, the signal intensity in the tumor is nearly four times that in the liver. These results suggest that compound **7** rapidly accumulates in tumor tissue and continues to stay bound to $\alpha_v\beta_3$ -expressing cancer cells despite partial clearing by the hepatobiliary system after 4 h. This rapid accumulation of compound **7** in the cancer cell is consistent with in vitro data aforementioned, which demonstrates **7** binding to the cancer cell membrane surface after 5 min. To further elucidate the accumulation of compound **7** in $\alpha_v\beta_3$ -expressing tumors in vivo, M21 tumor-bearing mice were injected with **7** and subsequently received a lateral tail vein injection of rhodamine-lectin 2 h later, just prior to euthanization. Rhodamine-lectin is used to delineate the vessels during the microscopic imaging. Tumors were

sectioned, mounted, and counterstained with DAPI and observed under a fluorescence microscope. The results are summarized in Figure 4 and they suggest the intracellular accumulation of compound **7** in $\alpha_v\beta_3$ -expressing cancer cells.

3. Conclusion

In conclusion, attachment of aliphatic carbamate linkers to integrin antagonist **1** resulted in a series of compounds with enhanced binding affinity to $\alpha_v\beta_3$. The neopentyl derivative **5a**, with the most lipophilic and bulky linker, was the most efficacious inhibitor of the series in both ELISA and cell adhesion assays. In addition, in vitro and in vivo data suggest compound **7** binds to and accumulates in $\alpha_v\beta_3$ -expressing tumor cells. Biodistribution data obtained from optical imaging of ex vivo tumors and various tissues also suggest the preferential binding of compound **7** in $\alpha_v\beta_3$ -expressing tumor cells even after partial hepatobiliary clearance. The terminal amine of compound **6a** can be functionalized to conjugate molecular beacons. Using the amine functionality in compound **6a**, integrin $\alpha_v\beta_3$ -targeted small molecule imaging probes for other imaging modalities including PET, SPECT, and MRI are currently being developed by conjugating appropriate molecular beacons to **6a**.

4. Experimental

4.1. General

All solvents and reagents were purchased from commercial sources and used without further purification. Infrared spectra were prepared as KBr pellets and recorded on a Perkin-Elmer Spectrum GX FT-IR spectrophotometer. ¹H NMR and ¹³C NMR data were recorded on a Bruker Ultrashield 300 instrument at 300 MHz for proton and 75 MHz for carbon using DMSO-*d*₆ or CDCl₃. Mass spectral data for compounds **4a–d** were recorded on a PE/SCIEX API 2000 instrument whereas high and low resolution mass spectral data for all other compounds were recorded on a JEOL JMS HX110 instrument using positive mode FAB with NBA (*meta*-nitro benzoic acid) matrix. Purified human integrin $\alpha_v\beta_3$ and purified human vitronectin were purchased from Chemicon International (Temecula, CA). *c*-[RGDfV] was purchased from Bachem Bioscience, Inc. (King of Prussia, PA) and was used as acquired. For in vitro assay screening, stock solutions of integrin antagonistic substances were prepared in anhydrous DMSO and diluted with purified water. Chemiluminescence for ELISA assays and A₅₉₀ for cell adhesion assays were recorded on a Wallac Victor² 1420 Multilabel Counter.

4.2. Representative procedure for synthesis of *N*-Boc-aminoalkyl-carbonyl-imidazoles

4.2.1. 3-(Boc-amino)-neopentyl-1-*O*-carbonylimidazole (4a). *N,N*-Diisopropylethylamine (1.7 mL, 9.85 mmol) was added to a stirred solution of **3a** (2.00 g, 9.85 mmol)

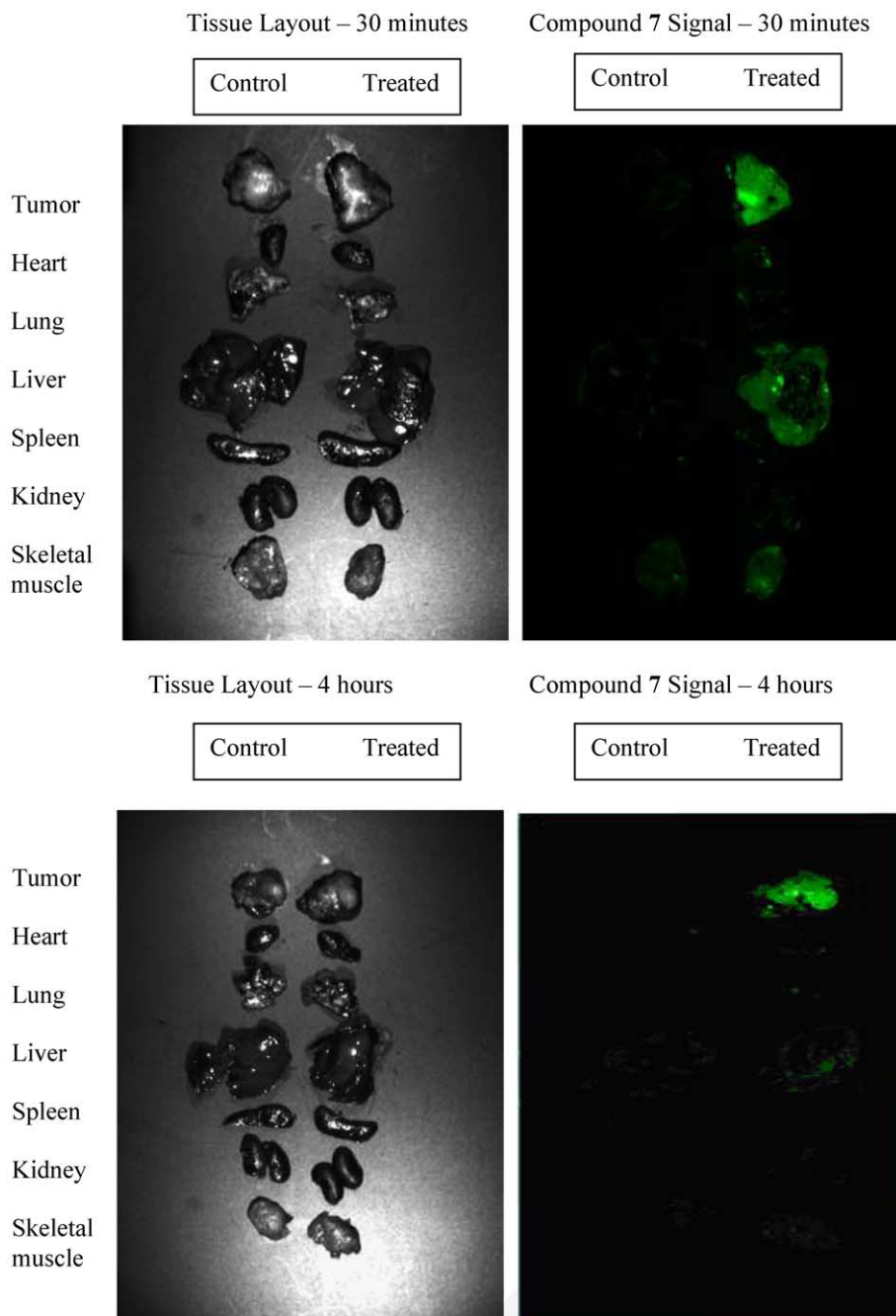


Figure 2. Biodistribution of compound 7 in ex vivo tissues. Imaging of excised tumors and organs 30 min and 4 h post-injection of compound 7 in M21 $\alpha_v\beta_3$ -expressing tumor-bearing mice. The organs include tumor, heart, lung, liver, spleen, kidney, and skeletal muscle. Compound 7 is excreted through the hepatobiliary and genitourinary system. Compound 7 retains signal in the tumor even after partial clearance through the hepatobiliary system at 4 h. Left panels show the tissue layout, right panels show the results from optical imaging.

in anhydrous CH_2Cl_2 (8 mL) under argon. To this solution, 1,1'-carbonyldiimidazole (2.80 g, 17.3 mmol) in CH_2Cl_2 (22 mL) was added as a slurry and this mixture was stirred at room temperature for 3 h. The mixture was diluted to 50 mL with CH_2Cl_2 , cooled to 0°C , and washed with ice-cold water (2×50 mL). The solvent was dried over Na_2SO_4 , evaporated under reduced pressure, and dried under high vacuum to give **4a** (2.72 g, 9.16 mmol, 93%) as a white solid. IR (KBr, cm^{-1}) 3367w, 3142m, 1759s, 1709s, 1474s, 1303s, 1179s, 1006m. ^1H NMR (300 MHz, $\text{DMSO}-d_6$): 8.28

(s, 1H), 7.61 (s, 1H), 7.08 (s, 1H), 7.00 (t, $J = 6.4$ Hz, 1H), 4.04 (s, 2H), 2.95 (d, $J = 6.4$ Hz, 2H), 1.35 (s, 9H), 0.92 (s, 6H). ^{13}C NMR (75 MHz, $\text{DMSO}-d_6$): 156.5, 148.8, 137.7, 130.6, 117.9, 78.0, 73.6, 47.2, 36.0, 28.6, 22.6. MS (electrospray): m/z 298 (100, $[\text{M}+\text{H}]^+$, calcd 298).

4.2.2. 2-(Boc-amino)-ethyl-1-O-carbonylimidazole (4b). White solid. Yield 90%. IR (KBr, cm^{-1}) 3403s, 2980m, 1748s, 1713s, 1526s, 1322s, 1166s, 1006m. ^1H NMR (300 MHz, $\text{DMSO}-d_6$): 8.27 (s, 1H), 7.61 (s, 1H), 7.15

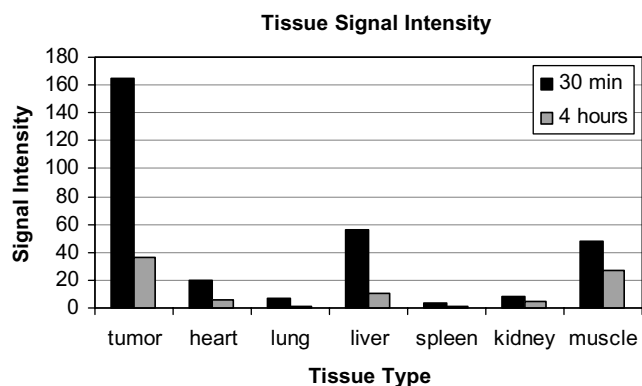


Figure 3. Qualitative data of the biodistribution of compound **7** in ex vivo tissues. Signal intensity was measured from images obtained of various ex vivo tissues, one animal for each time point, including tumor, heart, lung, liver, spleen, kidney, and skeletal muscle. Signal from compound **7** is most pronounced in $\alpha_v\beta_3$ -expressing tumor tissue at 30 min and 4 h post-injection even after clearance of signal from the liver due to hepatobiliary clearance.

(t, $J = 5.7$ Hz, 1H), 7.07 (s, 1H), 4.33 (t, $J = 5.1$ Hz, 2H), 3.33 (m, 2H), 1.36 (s, 9H). ^{13}C NMR (75 MHz, CDCl_3): 155.8, 148.6, 137.2, 130.7, 117.2, 80.0, 67.4, 39.4, 28.3. MS (electrospray): m/z 256 (100, $[\text{M}+\text{H}]^+$, calcd 256).

4.2.3. 3-(Boc-amino)-propyl-1-*O*-carbonylimidazole (4c). White solid. Yield 92%. IR (KBr, cm^{-1}) 3337s, 3141m, 2977m, 1753s, 1721s, 1520s, 1415m, 1160s, 1016m. ^1H NMR (300 MHz, $\text{DMSO}-d_6$): 8.27 (s, 1H), 7.60 (s, 1H), 7.08 (s, 1H), 6.94 (t, $J = 5.5$ Hz, 1H), 4.37 (t, $J = 6.2$ Hz, 2H), 3.09 (m, 2H), 1.84 (m, 2H), 1.35 (s, 9H). ^{13}C NMR (75 MHz, CDCl_3): 155.9, 148.7, 137.1, 130.5, 117.1, 79.5, 66.0, 37.1, 29.2, 28.3. MS (electrospray): m/z 270 (100, $[\text{M}+\text{H}]^+$, calcd 270).

4.2.4. 4-(Boc-amino)-butyl-1-*O*-carbonylimidazole (4d). Clear oil. Yield 90%. IR (KBr, cm^{-1}) 3407s, 2976m, 2934m, 1764s, 1712s, 1526s, 1475m, 1283s, 1174s, 1004m. ^1H NMR (300 MHz, $\text{DMSO}-d_6$): 8.26 (s, 1H), 7.60 (s, 1H), 7.08 (s, 1H), 6.84 (t, $J = 5.8$ Hz, 1H), 4.37 (t, $J = 6.3$ Hz, 2H), 2.97 (m, 2H), 1.72 (m, 2H), 1.51 (m, 2H), 1.37 (s, 9H). ^{13}C NMR (75 MHz,

$\text{DMSO}-d_6$): 156.1, 148.8, 137.6, 130.1, 117.9, 77.9, 68.3, 38.6, 28.7, 26.1, 25.7. MS (electrospray): m/z 284 (100, $[\text{M}+\text{H}]^+$, calcd 284).

4.3. Representative procedure for coupling IA **1** with *N*-Boc-aminoalkyl-carbonyl-imidazoles

4.3.1. 4-[2-(3,4,5,6-Tetrahydropyrimidin-2-ylamino)ethyl-oxy]benzoyl-2-(*S*)-[*N*-(3-butyloxycarbonylamino-neopentyl-1-carbamyl)]-aminoethylsulfonamino- β -alanine (5a). To a mixture of **4a** (0.42 g, 1.42 mmol) in anhydrous DMSO (12 mL) under argon, was added (0.50 g, 1.02 mmol) of **1**, as the hydrochloride salt, followed by addition of *N,N*-diisopropylethylamine (0.53 mL, 3.05 mmol). The mixture was stirred under argon at 70 °C for 18 h. Excess solvent was removed by rotary evaporation and the remaining residue was washed with water (2×5 mL) then with EtOAc (2×3 mL). The remaining solid was dissolved in hot EtOH, cooled and the resulting precipitate was collected by vacuum filtration then dried under high vacuum to give **5a** (0.65 g, 0.95 mmol, 66%) as an off-white solid. IR (KBr, cm^{-1}) 3323s, 3051m, 2973s, 2884m, 1704s, 1650s, 1607s, 1533m, 1505s, 1319s, 1146s, 1057m. ^1H NMR (300 MHz, $\text{DMSO}-d_6$): 8.86 (br, 1H), 8.58 (br, 2H), 8.29 (br, 1H), 7.73 (d, $J = 8.6$ Hz, 2H), 7.29 (t, $J = 5.3$ Hz, 1H), 7.02 (br, 1H), 6.92 (d, $J = 8.6$ Hz, 2H), 6.79 (t, $J = 5.8$ Hz, 1H), 4.04 (t, $J = 4.8$ Hz, 2H), 3.73 (m, 1H), 3.67 (s, 2H), 3.55 (m, 2H), 3.47 (m, 2H), 3.37 (t, $J = 7.0$ Hz, 2H), 3.24 (br, 4H), 3.18 (m, 2H), 2.82 (d, $J = 5.8$ Hz, 2H), 1.80 (m, 2H), 1.37 (s, 9H), 0.79 (s, 6H). ^{13}C NMR (75 MHz, $\text{DMSO}-d_6$): 173.5, 165.8, 160.8, 156.8, 156.5, 153.6, 129.2, 127.7, 114.5, 77.9, 70.5, 66.5, 56.6, 51.8, 47.5, 43.3, 38.4, 36.2, 35.9, 28.7, 22.6, 20.2, 15.6. MS (FAB, NBA): m/z 686 (100, $[\text{M}+\text{H}]^+$). HR-MS (FAB, NBA): m/z 686.3181 ($[\text{M}+\text{H}]^+$, $\text{C}_{29}\text{H}_{48}\text{N}_7\text{O}_{10}\text{S}$, calcd 686.3184).

4.3.2. 4-[2-(3,4,5,6-Tetrahydropyrimidin-2-ylamino)ethyl-oxy]benzoyl-2-(*S*)-[*N*-(2-butyloxycarbonylamino-ethyl-1-carbamyl)]-aminoethylsulfonamino- β -alanine (5b). White powder. Yield 23%. IR (KBr, cm^{-1}) 3380s, 3048w, 2976m, 2886w, 1702s, 1652s, 1607s, 1529m, 1367m, 1254s, 1056m. ^1H NMR (300 MHz, $\text{DMSO}-d_6$): 8.73 (br, 1H), 8.48 (br, 2H), 8.35 (br, 1H), 7.72 (d,

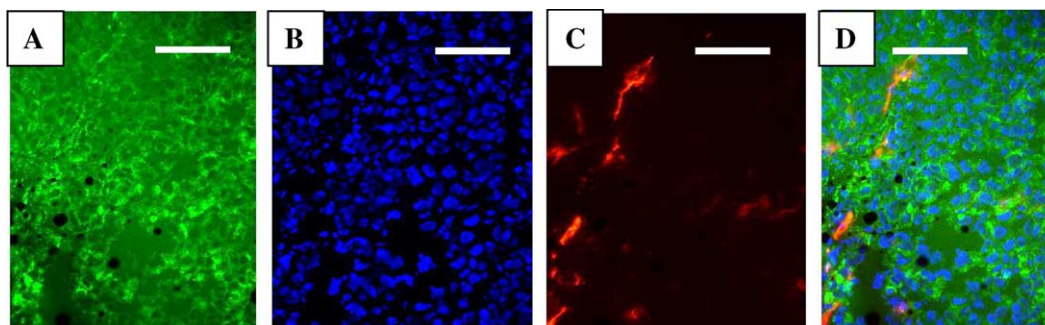


Figure 4. Bar represents 50 μM . Fluorescence microscopy of M21 $\alpha_v\beta_3$ -expressing tumors treated with compound **7**. M21 ($\alpha_v\beta_3$ expressing) tumor-bearing mice were injected with **7** and subsequently received a tail vein injection of rhodamine-lectin 2 h later, just prior to euthanization. Tumors were sectioned, mounted, and counterstained with DAPI and observed under a fluorescence microscope. Results suggest the intracellular accumulation of compound **7** in $\alpha_v\beta_3$ -expressing cancer cells. (A) Compound **7**; (B) DAPI; (C) rhodamine-lectin; (D) merge.

$J = 8.6$ Hz, 2H), 7.36 (t, $J = 5.9$ Hz, 1H), 6.96 (br, 1H), 6.92 (d, $J = 8.6$ Hz, 2H), 6.90 (t, $J = 5.8$ Hz, 1H), 4.04 (t, $J = 5.3$ Hz, 2H), 3.91 (t, $J = 5.5$ Hz, 2H), 3.63 (m, 1H), 3.55 (m, 2H), 3.47 (m, 2H), 3.34 (br, 2H), 3.24 (br, 4H), 3.16 (m, 2H), 3.11 (m, 2H), 1.81 (m, 2H), 1.37 (s, 9H). MS (FAB, NBA): m/z 644 (100, $[M+H]^+$). HR-MS (FAB, NBA): m/z 644.2716 ($[M+H]^+$, $C_{26}H_{42}N_7O_{10}S$, calcd 644.2714).

4.3.3. 4-[2-(3,4,5,6-Tetrahydropyrimidin-2-ylamino)ethyl-oxy]benzoyl-2-(S)-[N-(3-butyloxycarbonylamino-propyl-1-carbamyl)]-aminoethylsulfonfylamino- β -alanine (5c). Off-white powder. Yield 36%. IR (KBr, cm^{-1}) 3380s, 2976m, 2928m, 2881w, 1687m, 1647s, 1607s, 1504s, 1367m, 1255s, 1178m, 1054w. 1H NMR (300 MHz, DMSO- d_6): 9.07 (br, 1H), 8.67 (br, 2H), 8.28 (br, 1H), 7.72 (d, $J = 8.6$ Hz, 2H), 7.34 (t, $J = 5.3$ Hz, 1H), 7.01 (br, 1H), 6.90 (d, $J = 8.6$ Hz, 2H), 6.85 (t, $J = 5.5$ Hz, 1H), 4.02 (t, $J = 4.6$ Hz, 2H), 3.92 (t, $J = 6.2$ Hz, 2H), 3.67 (m, 1H), 3.55 (m, 2H), 3.47 (m, 2H), 3.34 (br, 2H), 3.23 (br, 4H), 3.18 (m, 2H), 2.96 (m, 2H), 1.80 (m, 2H), 1.63 (m, 2H), 1.37 (s, 9H). ^{13}C NMR (75 MHz, DMSO- d_6): 173.7, 165.7, 160.7, 156.6, 156.0, 153.7, 129.2, 127.7, 114.5, 78.0, 66.5, 62.3, 56.7, 51.6, 43.5, 38.4, 37.3, 35.9, 29.7, 28.7, 20.2 (21 of 22 resonances observed). MS (FAB, NBA): m/z 658 (100, $[M+H]^+$). HR-MS (FAB, NBA): m/z 658.2872 ($[M+H]^+$, $C_{27}H_{44}N_7O_{10}S$, calcd 658.2870).

4.3.4. 4-[2-(3,4,5,6-Tetrahydropyrimidin-2-ylamino)ethyl-oxy]benzoyl-2-(S)-[N-(4-butyloxycarbonylamino-butyl-1-carbamyl)]-aminoethylsulfonfylamino- β -alanine (5d). Off-white powder. Yield 33%. IR (KBr, cm^{-1}) 3380s, 3051w, 2975m, 2935m, 2874m, 1687m, 1647s, 1607s, 1504s, 1366m, 1255s, 1148m, 1055m. 1H NMR (300 MHz, DMSO- d_6): 9.06 (br, 1H), 8.66 (br, 2H), 8.28 (br, 1H), 7.72 (d, $J = 8.2$ Hz, 2H), 7.33 (t, $J = 5.1$ Hz, 1H), 6.98 (br, 1H), 6.90 (d, $J = 8.2$ Hz, 2H), 6.83 (t, $J = 5.5$ Hz, 1H), 4.02 (t, $J = 4.7$ Hz, 2H), 3.91 (t, $J = 5.9$ Hz, 2H), 3.66 (m, 1H), 3.55 (m, 2H), 3.46 (m, 2H), 3.41 (br, 2H), 3.23 (br, 4H), 3.18 (m, 2H), 2.90 (m, 2H), 1.80 (m, 2H), 1.49 (m, 2H), 1.47 (m, 2H), 1.36 (s, 9H). MS (FAB, NBA): m/z 672 (100, $[M+H]^+$). HR-MS (FAB, NBA): m/z 672.3029 ($[M+H]^+$, $C_{28}H_{46}N_7O_{10}S$, calcd 672.3027).

4.4. Representative procedure for deprotection of butyloxycarbonyl integrin antagonists

4.4.1. 4-[2-(3,4,5,6-Tetrahydropyrimidin-2-ylamino)ethyl-oxy]benzoyl-2-(S)-[N-(3-amino-neopenta-1-carbamyl)]-aminoethylsulfonfylamino- β -alanine hydrochloride (6a). A mixture of **5a** (0.10 g, 0.14 mmol) and 4 M HCl in dioxane (50 mL) was stirred under argon at 0 °C for 3 h. The heterogeneous mixture was frozen at -80 °C then lyophilized to dryness to give **6a** in quantitative yield as a hydrochloride salt. 1H NMR (300 MHz, DMSO- d_6): 12.97 (br, 1H), 8.49 (br, 1H), 7.99 (br, 2H), 7.95 (br, 2H), 7.88 (br, 1H), 7.84 (d, $J = 8.3$ Hz, 2H), 7.60 (t, $J = 5.1$ Hz, 1H), 7.40 (t, $J = 5.0$ Hz, 1H), 7.02 (d, $J = 8.3$ Hz, 2H), 4.12 (t, $J = 6.4$ Hz, 2H), 3.79 (s, 2H), 3.70 (m, 1H), 3.53 (m, 2H), 3.51 (br, 2H), 3.48 (m,

2H), 3.26 (br, 4H), 3.17 (m, 2H), 2.70 (br, 2H), 1.82 (m, 2H), 0.94 (s, 6H). MS (FAB, NBA): m/z 586 (100, $[M+H]^+$). HR-MS (FAB, NBA): m/z 586.2657 ($[M+H]^+$, $C_{24}H_{40}N_7O_8S$, calcd 586.2659).

4.4.2. 4-[2-(3,4,5,6-Tetrahydropyrimidin-2-ylamino)ethyl-oxy]benzoyl-2-(S)-[N-(2-amino-ethyl-1-carbamyl)]-aminoethylsulfonfylamino- β -alanine hydrochloride (6b). 1H NMR (300 MHz, DMSO- d_6): 12.97 (br, 1H), 8.50 (br, 1H), 8.06 (br, 2H), 7.97 (br, 2H), 7.90 (br, 1H), 7.84 (d, $J = 8.7$ Hz, 2H), 7.59 (t, $J = 5.5$ Hz, 1H), 7.21 (t, $J = 5.0$ Hz, 1H), 7.02 (d, $J = 8.7$ Hz, 2H), 4.14 (br, 2H), 4.12 (br, 2H), 3.70 (m, 1H), 3.53 (m, 2H), 3.51 (br, 2H), 3.49 (m, 2H), 3.26 (br, 4H), 3.17 (m, 2H), 3.03 (m, 2H), 1.82 (m, 2H). MS (FAB, NBA): m/z 544 (100, $[M+H]^+$). HR-MS (FAB, NBA): m/z 544.2187 ($[M+H]^+$, $C_{21}H_{34}N_7O_8S$, calcd 544.2189).

4.4.3. 4-[2-(3,4,5,6-Tetrahydropyrimidin-2-ylamino)ethyl-oxy]benzoyl-2-(S)-[N-(3-amino-propyl-1-carbamyl)]-aminoethylsulfonfylamino- β -alanine hydrochloride (6c). 1H NMR (300 MHz, DMSO- d_6): 12.96 (br, 1H), 8.50 (br, 1H), 7.95 (br, 2H), 7.91 (br, 2H), 7.87 (br, 1H), 7.83 (d, $J = 8.6$ Hz, 2H), 7.57 (t, $J = 5.1$ Hz, 1H), 7.29 (t, $J = 4.9$ Hz, 1H), 7.02 (d, $J = 8.6$ Hz, 2H), 4.12 (t, $J = 4.7$ Hz, 2H), 4.01 (t, $J = 5.5$ Hz, 2H), 3.70 (m, 1H), 3.55 (m, 2H), 3.50 (br, 2H), 3.48 (m, 2H), 3.26 (br, 4H), 3.15 (m, 2H), 2.84 (m, 2H), 1.84 (m, 2H), 1.82 (m, 2H). MS (FAB, NBA): m/z 558 (100, $[M+H]^+$). HR-MS (FAB, NBA): m/z 558.2344 ($[M+H]^+$, $C_{22}H_{36}N_7O_8S$, calcd 558.2346).

4.4.4. 4-[2-(3,4,5,6-Tetrahydropyrimidin-2-ylamino)ethyl-oxy]benzoyl-2-(S)-[N-(4-amino-butyl-1-carbamyl)]-aminoethylsulfonfylamino- β -alanine hydrochloride (6d). 1H NMR (300 MHz, DMSO- d_6): 12.96 (br, 1H), 8.50 (br, 1H), 8.02 (br, 2H), 7.95 (br, 2H), 7.88 (br, 1H), 7.84 (d, $J = 8.6$ Hz, 2H), 7.63 (t, $J = 5.7$ Hz, 1H), 7.22 (t, $J = 5.3$ Hz, 1H), 7.01 (d, $J = 8.6$ Hz, 2H), 4.12 (br, 2H), 3.95 (br, 2H), 3.68 (m, 1H), 3.54 (m, 2H), 3.51 (br, 2H), 3.48 (m, 2H), 3.26 (br, 4H), 3.15 (m, 2H), 2.79 (m, 2H), 1.81 (m, 2H), 1.66 (m, 2H), 1.61 (m, 2H). MS (FAB, NBA): m/z 572 (100, $[M+H]^+$). HR-MS (FAB, NBA): m/z 572.2507 ($[M+H]^+$, $C_{23}H_{38}N_7O_8S$, calcd 572.2502).

4.5. 4-[2-(3,4,5,6-Tetrahydropyrimidin-2-ylamino)ethyl-oxy]benzoyl-2-(S)-[N-(3-amino-neopenta-1-carbamyl)]-aminoethylsulfonfylamino- β -alanine fluorescein thiourea (7)

To a mixture of **6a** (0.11 g, 0.17 mmol) in anhydrous DMSO (10 mL) under argon, was added *N,N*-diisopropylethylamine (0.06 mL, 0.34 mmol) followed by addition of fluorescein isothiocyanate (0.07 g, 0.19 mmol). This mixture was stirred under argon at 40 °C for 18 h. Excess solvent was removed by rotary evaporation and the remaining residue was purified by reverse phase HPLC (4:1 MeOH-H₂O, 1 mL/min, t_R 10.5 min, C18 Microsorb, Varian, Inc.). The collected fractions were combined and excess solvent was removed by rotary evaporation followed by high vacuum to give **7**

(0.04 g, 0.04 mmol, 24%) as a dark orange powder. ^1H NMR (300 MHz, MeOD- d_4): 8.18 (s, 1H), 7.83 (d, $J = 8.0$ Hz, 1H), 7.68 (d, $J = 8.5$ Hz, 2H), 7.11 (d, $J = 8.0$ Hz, 1H), 7.10 (m, 2H), 6.82 (d, $J = 8.5$ Hz, 2H), 6.50 (s, 2H), 6.49 (m, 2H), 4.02 (t, $J = 6.0$ Hz, 1H), 3.92 (t, $J = 4.5$ Hz, 2H), 3.89 (s, 2H), 3.83 (m, 2H), 3.74 (s, 2H), 3.68 (d, $J = 6.0$ Hz, 2H), 3.62 (br, 2H), 3.43 (t, $J = 5.9$ Hz, 2H), 3.18 (t, $J = 5.6$ Hz, 4H), 1.85 (m, 2H), 1.05 (s, 6H). MS (electrospray): m/z 1020 (100, $[\text{M}+2\text{Na}-\text{H}]^+$), m/z 973 (100, $[\text{M}-\text{H}]^-$). HR-MS (FAB, NBA): m/z 975.3021 ($[\text{M}+\text{H}]^+$, $\text{C}_{45}\text{H}_{50}\text{N}_{13}\text{O}_8\text{S}_2$, calcd 975.2939).

4.6. In vitro assay procedures

4.6.1. ELISA. Purified integrin $\alpha_v\beta_3$ protein (Chemicon International, Temecula, CA) was applied to 96-well polystyrene microtiter plates at 0.1 $\mu\text{g}/\text{well}$. After overnight incubation at 4 °C the plates were washed, and then blocked with milk solution (KPL, Inc., Gaithersburg, MD) at room temperature for 2 h. The blocking buffer was removed, and the plates were inoculated in quadruplicate with integrin antagonistic substances with a typical starting concentration of 1.25 μM . Serial dilutions were prepared in the 96-well plates using multi-channel pipettes. To each well was added biotinylated vitronectin solution (0.1 $\mu\text{g}/\text{well}$) as standard competitor. The plates were incubated at room temperature for 3 h, washed, and the bound vitronectin was detected using NeutrAvidin-HRP conjugate at 0.01 $\mu\text{g}/\text{well}$ (Pierce, Rockford, IL) and LumiGlo chemiluminescent substrate system (KPL, Inc., Gaithersburg, MD). The luminescence was read using a Wallac Counter. The concentration of inhibitor producing 50% inhibition (IC_{50}) of vitronectin binding to $\alpha_v\beta_3$ was calculated based on a curve fitting model using KaleidaGraph 3.5 (Synergy Software, Reading, PA).

4.6.2. Cell adhesion assay. Integrin antagonistic substances were incubated with human melanoma M21 cells expressing $\alpha_v\beta_3$ integrin proteins on their surface. At a starting concentration of 0.5 mM, serial dilutions of the integrin antagonist/cell culture mixture were added to 96-well plates previously coated with purified human vitronectin (Chemicon International, Temecula, CA) and blocked with BSA. After incubation at 30 °C for 1 h, the plates were washed with distilled water to remove the unbound cells. The bound cells were then stained with 0.05% Crystal Violet, washed again with distilled water, and lysed with 1% SDS. Absorption @ 590 nm was measured on a Wallac Counter and the concentration of inhibitor producing 50% inhibition (IC_{50}) of vitronectin binding to $\alpha_v\beta_3$ is calculated based on a curve fitting model using KaleidaGraph 3.5 (Synergy Software, Reading, PA).

4.6.3. Cell uptake assay. M21 human melanoma cells expressing $\alpha_v\beta_3$ were cultured in glass chambers. Cells were given fresh media 30 min prior to treatment. Compound 7 (500 μL , 50 $\mu\text{g}/\text{mL}$) was added to each glass chamber and left to incubate for 5 min. Cells were washed with warm PBS three times and subsequently

mounted, counterstained with DAPI and observed under a fluorescence microscope. Negative control chambers were given the same concentration of FITC only.

4.7. In vivo procedures

4.7.1. Animal protocols. All studies were conducted in compliance with the National Institutes of Health Clinical Center Animal Use and Care Committee's requirements for the care and use of laboratory animals in research. The human melanoma (M21, received from Dr. David Cheresch of Scripps Research Institutes, La Jolla, CA) expressing $\alpha_v\beta_3$ was induced by subcutaneous injection in the right flank. Palpable masses were detected at 14–21 days post implant. The animals were manually restrained during tail vein injection. All tail vein injections were carried out with a 30 gauge needle placed in a lateral tail vein. Each animal weighing about 18–20 g received 100 μL of a 6 mg/mL solution of compound 7. In experiments where animals were given a rhodamine-lectin injection to outline tumor vasculature, mice were given 250 μL of rhodamine-lectin (5 mg/mL) through the lateral tail vein.

4.7.2. Imaging procedure. A simple noninvasive in vivo multispectral fluorescence imaging apparatus employed to assess the localization and distribution of various fluorophores has been previously described.²⁹ Laser light of the appropriate incident wavelength to excite the fluorophore was launched into a fiber optic bundle. A defocusing lens in position after the bundle expanded the beam such that the entire mouse was illuminated. An argon laser excited the fluorescein compound at the appropriate wavelength of 494 nm and a 515 nm long pass filter was used to detect all emissions past 515 nm up to 950 nm. The detector was a CRI, Inc. Maestro CCD camera. An interference filter in front of the CCD (515 nm for fluorescein) allowed for detection of the emitted fluorescent light only. Images were acquired and processed using Maestro acquisition and analysis software from CRI, Inc. Typically, control and treated ex vivo tumor and organ tissue was imaged concurrently under fixed settings. Data analysis consisted of subtracting (pixel by pixel) background auto fluorescence in control tissues from treated tissue in the same image and displaying the results in gray scale or false color. Semi-quantitative data were obtained by using ImageJ analysis software to semi-quantitate the signal intensity values recorded in Maestro acquisition and analysis software.

Acknowledgements

We would like to thank Dr. David Cheresch of Scripps Research Institutes, La Jolla, CA for kindly providing the M21 cells and the Michigan State University Mass Spectrometry Facility for low and high resolution mass spectral analysis of integrin antagonist compounds. J.Q. would like to thank the Howard Hughes Medical Institute—National Institutes of Health Research Scholars Program for their support.

References and notes

1. Takagi, J.; Springer, T. A. *Immunol. Rev.* **2002**, *186*, 141–163.
2. Humphries, M. J. *Biochem. Soc. Trans.* **2000**, *28*, 311–339.
3. Arnaout, M. A. *Immunol. Rev.* **2002**, *186*, 125–140.
4. Yamada, K. M.; Geiger, B. *Curr. Opin. Cell Biol.* **1997**, *9*, 76–85.
5. Calderwood, D. A.; Shattil, S. J.; Ginsberg, M. H. *J. Biol. Chem.* **2000**, *275*, 22607–22610.
6. (a) Plow, E. F.; Haas, T. A.; Zhang, L.; Loftus, J.; Smith, J. W. *J. Biol. Chem.* **2000**, *275*, 21785–21788; (b) Xiong, J.-P.; Stehle, T.; Zhang, R.; Dunker, R.; Joachimiak, A.; Frech, M.; Goodman, S. L.; Arnaout, M. A. *Science* **2002**, *296*, 151–155.
7. Rodan, S. B.; Rodan, G. A. *J. Endocrinol.* **1997**, *154*, S47–S56.
8. Storgard, C. M.; Stupack, D. G.; Jonczyk, A.; Goodman, S. L.; Fox, R. I.; Cheresch, D. A. *J. Clin. Invest.* **1999**, *103*, 47–54.
9. Friedlander, M.; Theesfeld, C. L.; Sugita, M.; Fruttinger, M.; Thomas, M. A.; Chang, S.; Cheresch, D. A. *Proc. Natl. Acad. Sci. U.S.A.* **1996**, *93*, 9764–9769.
10. (a) Eliceiri, B. P.; Cheresch, D. A. *J. Clin. Invest.* **1999**, *103*, 1227–1230; (b) Brooks, P. C.; Clark, R. A.; Cheresch, D. A. *Science* **1994**, *264*, 569–571.
11. Guerrero, C. A.; Méndez, E.; Zárate, S.; Isa, P.; López, S.; Arlas, C. F. *Proc. Natl. Acad. Sci. U.S.A.* **2000**, *97*, 14644–14649.
12. Wickham, T. J.; Mathias, P.; Cheresch, D. A.; Nemerow, G. R. *Cell* **1993**, *73*, 309–319.
13. (a) Pierschbacher, M. D.; Ruoslahti, E. *Nature* **1984**, *309*, 30–33; (b) Ruoslahti, E.; Pierschbacher, M. D. *Cell* **1986**, *44*, 517–518.
14. (a) Haubner, R.; Gratias, R.; Diefenbach, B.; Goodman, S. L.; Jonczyk, A.; Kessler, H. *J. Am. Chem. Soc.* **1996**, *118*, 7461–7472; (b) Duggan, M. E.; Hutchinson, J. H. *Exp. Opin. Ther. Pat.* **2000**, *10*, 1367–1383.
15. (a) Folkman, J. *Nat. Med.* **1995**, *1*, 27–31; (b) Schnitzer, J. E. *N. Engl. J. Med.* **1998**, *339*, 472–474; (c) Arap, W.; Pasqualini, R.; Ruoslahti, E. *Science* **1998**, *279*, 377–380.
16. (a) Coleman, P. J.; Brashear, K. M.; Askew, B. C.; Hutchinson, J. H.; McVean, C. A.; Duong, L. T.; Feuston, B. P.; Fernandez-Metzler, C.; Gentile, M. A.; Hartman, G. D.; Kimmel, D. B.; Leu, C.-T.; Lipfert, L.; Merkle, K.; Pennypacker, B.; Prueksaritanont, T.; Rodan, G. A.; Wesolowski, G. A.; Rodan, S. B.; Duggan, M. E. *J. Med. Chem.* **2004**, *47*, 4829–4837; (b) Hutchinson, J. H.; Halczenko, W.; Brashear, K. M.; Breslin, M. J.; Coleman, P. J.; Duong, L. T.; Fernandez-Metzler, C.; Gentile, M. A.; Fisher, J. E.; Hartman, G. D.; Huff, J. R.; Kimmel, D. B.; Leu, C.-T.; Meissner, R. S.; Merkle, K.; Nagy, R.; Pennypacker, B.; Perkins, J. J.; Prueksaritanont, T.; Rodan, G. A.; Varga, S. L.; Wesolowski, G. A.; Zartman, A. E.; Rodan, S. B.; Duggan, M. E. *J. Med. Chem.* **2003**, *46*, 4790–4798; (c) Engleman, V. W.; Nickols, G. A.; Ross, F. P.; Horton, M. A.; Griggs, D. W.; Settle, S. L.; Ruminski, P. G.; Teitelbaum, S. L. *J. Clin. Invest.* **1997**, *99*, 2284–2292.
17. (a) Eskens, F. A. L. M. *Br. J. Cancer* **2004**, *90*, 1–7; (b) Buerkle, M. A.; Pahernik, S. A.; Sutter, A.; Jonczyk, A.; Messmer, K.; Dellian, M. *Br. J. Cancer* **2002**, *86*, 788–795.
18. Eliceiri, B. *Circ. Res.* **2001**, *89*, 1104–1110.
19. Hood, J. D.; Bednarski, M.; Frausto, R.; Guccione, S.; Reisfeld, R. A.; Xiang, R.; Cheresch, D. A. *Science* **2002**, *296*, 2404–2407.
20. (a) Haubner, R.; Wester, H.-J.; Weber, W. A.; Mang, C.; Ziegler, S. I.; Goodman, S. L.; Senekowitsch-Schmidtko, R.; Kessler, H.; Schwaiger, M. *Cancer Res.* **2001**, *61*, 1781–1785; (b) Ogawa, M.; Hatano, K.; Oishi, S.; Kawasumi, Y.; Fujii, N.; Kawaguchi, M.; Doi, R.; Imamura, M.; Yamamoto, M.; Ajito, K.; Mukai, T.; Saji, H.; Ito, K. *Nucl. Med. Biol.* **2003**, *30*, 1–9.
21. (a) Harris, T. D.; Kalogeropoulos, S.; Nguyen, T.; Liu, S.; Bartis, J.; Ellars, C.; Edwards, S.; Onthank, D.; Silvia, P.; Yalamanchili, P.; Robinson, S.; Lazewatsky, J.; Barrett, J.; Bozarth, J. *Cancer Biother. Radiopharm.* **2003**, *18*, 627–641; (b) Liu, S.; Harris, T. D.; Ellars, C. E.; Edwards, D. S. *Bioconjugate Chem.* **2003**, *14*, 1030–1037; (c) Onthank, D. C.; Liu, S.; Silva, P. J.; Barrett, J. A.; Harris, T. D.; Robinson, S. P.; Edwards, D. S. *Bioconjugate Chem.* **2004**, *15*, 235–241.
22. (a) Sipkins, D. A.; Cheresch, D. A.; Kazemi, M. R.; Nevin, L. M.; Bednarski, M. D.; Li, K. C. P. *Nat. Med.* **1998**, *4*, 623–626; (b) Winter, P. M.; Caruthers, S. D.; Kassner, A.; Harris, T. D.; Chinen, L. K.; Allen, J. S.; Lacy, E. K.; Zhang, H.; Robertson, J. D.; Wickline, S. A.; Lanza, G. M. *Cancer Res.* **2003**, *63*, 5838–5843.
23. (a) Bloch, S.; Liang, K.; Dorshow, R. B.; Ye, Y.; Achilefu, S. I. *Proc. SPIE* **2004**, *5329*, 222–228; (b) Wang, W.; Ke, S.; Wu, Q.; Charnsangavej, C.; Gurfinkel, M.; Gelovani, J. G.; Abbuzzese, J. L.; Sevick-Muraca, E. M.; Li, C. *Mol. Imaging* **2004**, *3*, 343–351; (c) Chen, X.; Conti, P. S.; Moats, R. A. *Cancer Res.* **2004**, *64*, 8009–8014.
24. Duggan, M. E.; Duong, L. T.; Fisher, J. E.; Hamill, T. G.; Hoffman, W. F.; Huff, J. R.; Ihle, N. C.; Leu, C.-T.; Nagy, R. M.; Perkins, J. J.; Rodan, S. B.; Wesolowski, G.; Whitman, D. B.; Zartman, A. E.; Rodan, G. A.; Hartman, G. D. *J. Med. Chem.* **2000**, *43*, 3736–3745.
25. Enschede, C.; Hesse, M. *Helv. Chim. Acta* **2003**, *86*, 233–246.
26. (a) Blaszykowski, C.; Dhiman, A.-L.; Fensterbank, L.; Malacria, M. *Org. Lett.* **2003**, *5*, 1341–1344; (b) Mattingly, P. G. *Synthesis* **1990**, *4*, 366–368; (c) Gray, C. J.; Parker, R. C. *Tetrahedron* **1975**, *31*, 2940–2943; (d) Lee, B. H.; Miller, M. J. *J. Org. Chem.* **1983**, *48*, 24–31.
27. The chiral purity of the deprotected compounds **6a–d** is currently under investigation.
28. Achilefu, S.; Jimenez, H. N.; Dorshow, R. B.; Bugaj, J. E.; Webb, E. G.; Wilhelm, R. R.; Rajagopalan, R.; Johler, J.; Erion, J. L. *J. Med. Chem.* **2002**, *45*, 2003–2015.
29. Levenson, R.; Mansfield, J. R. Abstract ID 184, The Thrid Annual Meeting of the Society of Molecular Imaging, Sep 9–12, 2004.